Toxicology Reports 2 (2015) 27–39

Contents lists available at ScienceDirect

Toxicology Reports

journal homepage: www.elsevier.com/locate/toxrep

In vitro toxicity assessment of chitosan oligosaccharide coated iron oxide nanoparticles

Sudeep Shukla[a,*], Alka Jadaun[b], Vikas Arora[c], Raj Kumar Sinha[d], Neha Biyani[e], V.K. Jain[a]

[a] School of Environmental Sciences, Jawaharlal Nehru University, New Delhi 110067, India
[b] School of Biotechnology, Jawaharlal Nehru University, New Delhi 110067, India
[c] Department of Chemistry, Indian Institute of Technology, New Delhi 110016, India
[d] Centre for Biomedical Engineering, Indian Institute of Technology, New Delhi 110016, India
[e] School of Life Sciences, Jawaharlal Nehru University, New Delhi 110067, India

ARTICLE INFO

Article history:
Received 25 June 2014
Received in revised form
25 September 2014
Accepted 1 November 2014
Available online 7 November 2014

Keywords:
Iron oxide nanoparticles
Chitosan oligosaccharide
Cytotoxicity

ABSTRACT

Iron oxide nanoparticles (INPs) have potential biological, biomedical and environmental applications. These applications require surface modification of the iron oxide nanoparticles, which makes it non-toxic, biocompatible, stable and non-agglomerative in natural and biological surroundings. In the present study, iron oxide nanoparticles (INPs) and chitosan oligosaccharide coated iron oxide nanoparticles (CSO-INPs) were synthesized to evaluate the effect of surface coating on the stability and toxicity of nanoparticles. Comparative *in vitro* cytotoxicity of nanoparticles was evaluated in HeLa (human cervix carcinoma), A549 (human lung carcinoma) and Hek293 (human embryonic kidney) cells by using 3-(4,5-dimethylthiazol-2-yl)-2,5-diphenyltetrazolium bromide (MTT) assay along with flow cytometry study for cell viability, membrane integrity, mitochondrial membrane potential (MMP) and reactive oxygen species (ROS) production. Morphological alteration in nanoparticles treated cells was analyzed by Acridine orange/ethidium bromide double staining and electron microscopy. Synthesized nanoparticles were found to be spherical in shape, well dispersed and stable at various pH values, making them suitable for biomedical and environmental applications. The present study also indicates that the chitosan oligosaccharide coating on iron oxide nanoparticles results in the decrease in cellular damage and moderate ROS production, thereby, significantly decreasing the cytotoxic impact of bare iron oxide nanoparticles.

1. Introduction

Nanoscience has emerged as an innovative research field having application in a number of scientific and technological areas, including materials science, electronics, biotechnology and medical sciences [1]. Nanomaterials can be found in more than 1000 consumer products including electronic components, cosmetics, antimicrobial and stain-resistant fabric cleaning products [2,3]. Among the nanostructured materials, metallic nanoparticles in particular, iron oxide nanoparticles have been the focus of intensive research. Magnetic iron oxide nanoparticles have potential applications in various disciplines of science ranging from environmental remediation to biomedical such as magnetic drug targeting, tissue repair, and cell tissue targeting [4].

* Corresponding author. Tel.: +91 9873674030.
E-mail addresses: sudeepshukla@gmail.com, sudeepshukla@rediffmail.com (S. Shukla).

http://dx.doi.org/10.1016/j.toxrep.2014.11.002

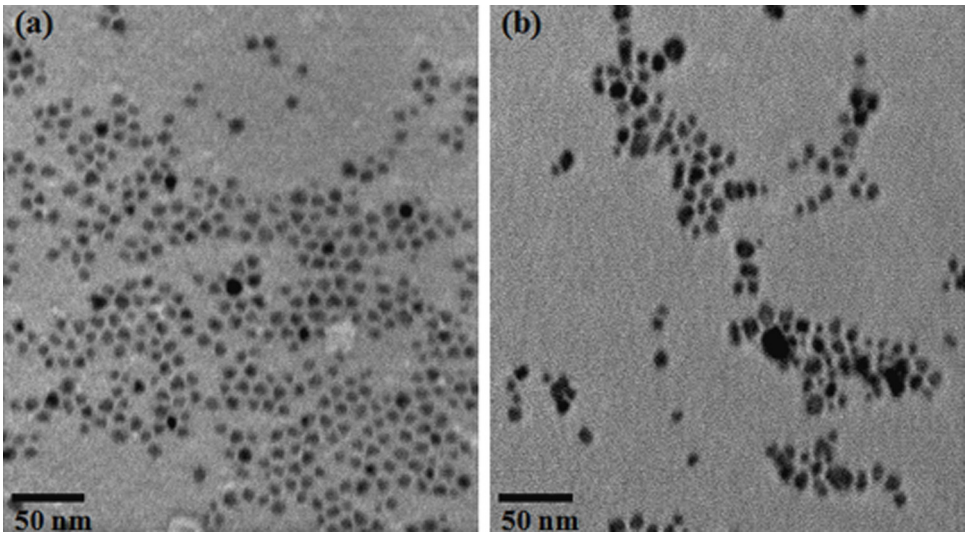

Fig. 1. TEM image of iron oxide nanoparticles (INPs) (a). TEM image of chitosan oligosaccharide coated iron oxide nanoparticles (CSO-INP) (b).

Magnetic iron oxide nanoparticles with a bare surface tend to agglomerate because of strong magnetic attractions among the particles. Stabilizers such as carboxylates, inorganic compounds and polymeric compounds have functional groups to modify these particles and enhance its stability [5,6]. Among the various polymers, chitosan an alkaline product of chitin has been widely examined due to its hydrophilicity, biocompatibility and biodegradability [7,8]. Chemically chitosan is insoluble in water and behaves as a weak base making it inappropriate for biological and environmental applications. On the other hand, chitosan oligosaccharides, which can be produced by degradation of chitosan polymer chain, are water soluble making it suitable for biological and environmental applications [9].

Previous studies have highlighted the potential environmental and health hazards caused by nanomaterials [10–13]. Nanoscale properties such as high surface to volume ratio, high surface energy, and higher surface reactivity may imperil human health through cytotoxic and genotoxic effects [13].

Nanomaterials can enter the human body through dermal absorption, respiratory inhalation, or oral route. Due to their ultrafine size, they are able to move across the olfactory mucosa, alveolar membrane and capillary endothelium. The ability of nanomaterials to cross blood brain barrier enhances its toxicity for the nervous system [14].

There is an urgent need for understanding the potential risks associated with iron oxide nanoparticles along with the range of surface coatings utilized for its functionality [15–17]. Earlier published reports corroborate the probable mechanism of internalization and interaction of iron oxide nanoparticles with various cellular targets mainly mitochondria, nucleus and DNA [18,19].

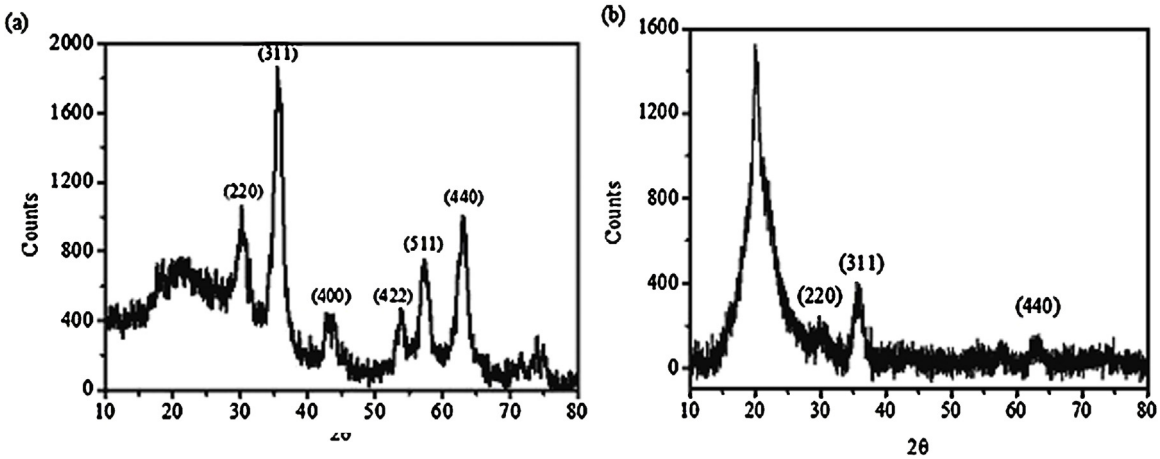

Fig. 2. X-ray diffraction (XRD) pattern of iron oxide nanoparticles (INPs) (a). X-ray diffraction (XRD) pattern of chitosan oligosaccharide coated iron oxide nanoparticles (CSO-INPs) (b).

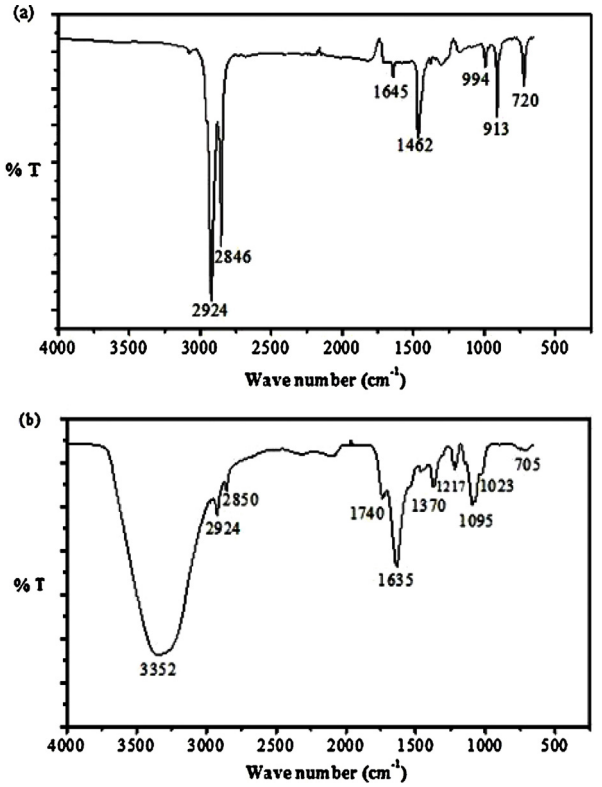

Fig. 3. Fourier transform infrared (FTIR) spectroscopy characteristic peaks of iron oxide nanoparticles (INPs) (a). FTIR characteristic peaks of chitosan oligosaccharide coated iron oxide nanoparticles (CSO-INPs) (b).

In this study, bare iron oxide nanoparticles and chitosan oligosaccharide coated iron oxide nanoparticles were synthesized and characterized by transmission electron microscopy (TEM), Fourier transform infrared (FTIR) spectroscopy, X-ray diffraction (XRD), zeta potential analysis and physical property measurement system (PPMS). Thereafter, comparative toxicity assessment of nanoparticles (INPs and CSO-INPs) was performed on three cell lines (HeLa, A549 and Hek293) by MTT assay (cell viability). We then evaluated the toxicity mechanism of nanoparticles and inferred the influence of surface engineering on cell toxicity by various cytotoxic assays: phosphatidylserine exclusion assay (mitochondria membrane integrity), JC-1 probe staining (mitochondria membrane potential), DCFH-DA assay (estimation of ROS generation) and DHE assay (DNA degradation estimation). Along with above explained assays, morphological changes in cellular targets were corroborated by Acridine orange/ethidium bromide double staining and electron microscopy.

2. Materials and methods

2.1. Chemicals

Analytical grade chemicals, iron (III) chloride (97%), oleic acid (90%), n-hexane (95%), anhydrous ethanol, 1-octadecene (90%), acetic acid, 1-ethyl-3-(3-dimethylamino-propyl)-N-ethylcarbodiimide hydrochloride (EDC)

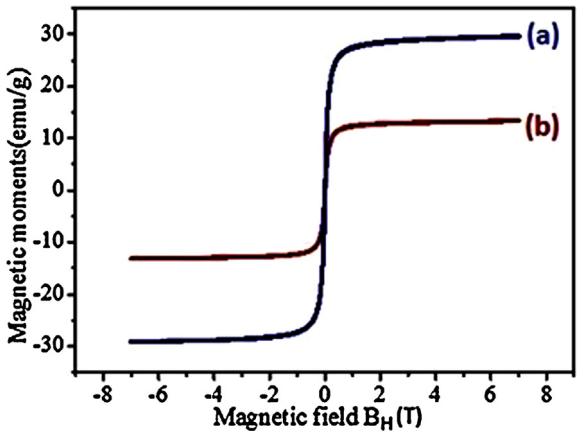

Fig. 4. Hysteresis loop of iron oxide nanoparticles (INPs) at 300 K (a). Chitosan oligosaccharide coated iron oxide nanoparticles (CSO-INPs) (b).

(commercial grade), N-hydroxy-succinimide (NHS), chitosan oligosaccharide (Mn 5000 and >90% deacetylated), JC-1 (5,5,6,6-tetrachloro-1,1,3,3-tetraethyl-benzimidazolylcarbocyanineiodide), dihydrochlorofluorescein-diacetate (DCFH-DA) and dihydroethidine (DHE), Annexin V-FITC, ethidium bromide and trypsin–EDTA (ethylenediamine tetra acetic acid) were purchased from Sigma–Aldrich. N-[(3-trimethoxysilyl) propyl] EDTA trisodium salt (50% in water) was received from Gelest Inc., U.S.A. The water used throughout this work was of reagent grade produced by a Milli-Q water purification system. DMEM (Dulbecco's modified Eagle's medium), FBS (foetal bovine serum) and PenStrep (penicillin–streptomycin) were purchased from Biological Industries Inc.

2.2. Synthesis of nanoparticles

2.2.1. Synthesis of iron oxide nanoparticles (INPs)

Fe_3O_4 nanoparticles were synthesized as described by Jana et al. [20] with slight modifications. In a typical synthesis of iron–oleate complex, 2.55 g of iron chloride ($FeCl_3{\cdot}6H_2O$) was dissolved in 100 ml of methanol and 11 ml of oleic acid under continuous stirring. Another solution prepared by dissolving 1.6 g of NaOH in 200 ml of methanol was added to the above solution in stirring condition. The observed brown precipitate of iron oleate was washed with methanol and dried under vacuum overnight to remove the solvent. 4.02 g of synthesized solid mass was dissolved in 30 ml of 1-octadecene at 70 °C to make stock solution. Thereafter, 10 ml of stock solution was mixed with 40 ml of 1-octadecene and 0.1 equiv. of oleic acid and the solution was heated to 280 °C for 30 min in an inert environment. When the reaction was complete, the mixture was precipitated twice with ethanol. Resulting precipitate was re-dispersed in hexane for further use.

2.2.2. Synthesis of chitosan oligosaccharide linked iron oxide nanoparticles (CSO-INPs)

Synthesized nanoparticles are stable in nonpolar solvents (such as hexane) and capped with nonpolar end groups on their surface. Oleic acid is widely used in the synthesis of iron oxide nanoparticles because it can

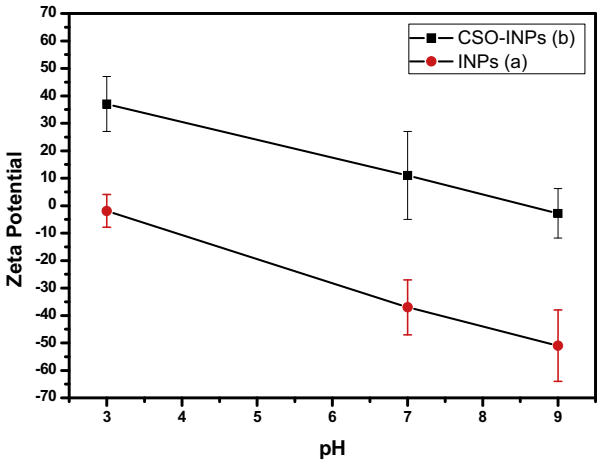

Fig. 5. Zeta potential measurement of iron oxide nanoparticles (a). Chitosan oligosaccharide coated iron oxide nanoparticles (b) at pH 3, 7 and 9.

form a dense protective monolayer, thereby, producing highly uniform and monodisperse particles [6]. For the synthesis of iron oxide nanoparticles (INPs) suitable for biological applications, the hydrophobic surfactant coating needs to be replaced by a hydrophilic, biocompatible, and functional coating that allows controlled interaction of nanoparticles with biological species. The oleic acid on the particle surface was replaced with a —COOH containing silane using a method reported by Palma et al. [21]. Once functionalized with a carboxylic group, nanoparticles were further functionalized using chitosan oligosaccharide method developed by López-Cruz et al. [22]. Amino group of chitosan oligosaccharide was covalently bonded with terminal carboxylic group of silane functionalized iron oxide nanoparticles through carbodiimide activation by the reaction of EDC and NHS [23].

2.2.3. Characterization of chitosan linked iron oxide nanoparticles (CSO-INPs)

TEM images were recorded on a JEOL 2100F TEM, operated at an accelerating voltage of 200 kV. Samples were prepared by adding 10 μl of the nanoparticles solution on 200-mesh carbon coated Cu grids. For the rapid counting of nanoparticles, TEM images were further processed by NIH Image J software [24]. Powder X-ray diffraction (XRD) studies were carried out through a Philips1820 advance diffractometer equipped with Ni-filtered Cu Kα radiation maintaining the scan rate of 0.24° per minute. Fourier transform infrared (FTIR) spectroscopy studies were carried out by Varian 7000 FTIR to determine the chemical functional groups in the nanoparticles at various steps of synthesis.

FTIR spectra were recorded in the range of 500–4000 cm^{-1} with an average of 16 scans per sample. Physical property measurement system (PPMS, Cryogenic PT 415) magnetometer was used to measure the magnetization of synthesized nanoparticles. A known amount of the dry powder of nanoparticles was loaded in sample capsule and suspended in magnetometer.

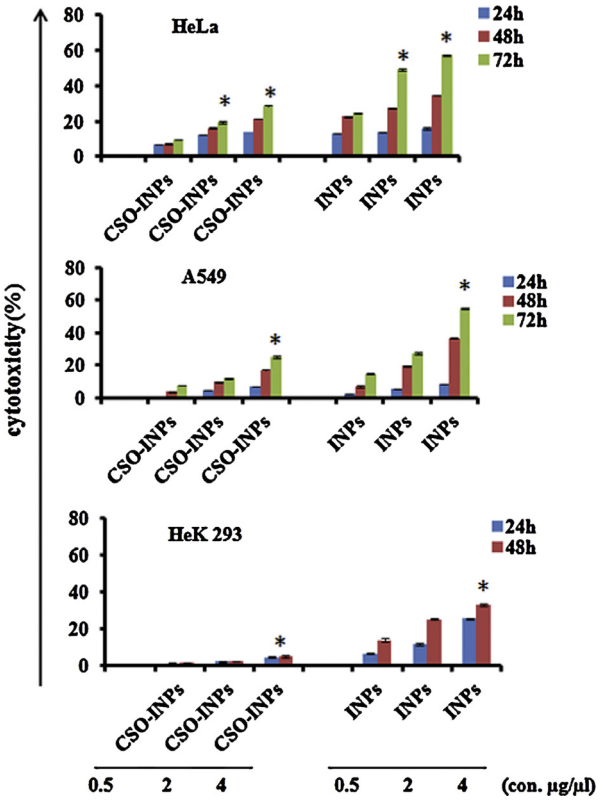

Fig. 6. Representation of cytotoxicity of iron oxide nanoparticles (INPs) and chitosan oligosaccharide coated iron oxide nanoparticles (CSO-INPs) in HeLa, A549 and Hek293 cells, with different concentrations at various time intervals. Statistical analysis was performed by Student's *t*-test followed by three independent experiments, the statistical significance of INPs shown in error bars represents the standard error mean, $^{*}p < 0.05$.

Magnetization of sample was measured with respect to variable magnetic field −0.7 T to +0.7 T at 300 K.

2.3. In vitro toxicity studies

2.3.1. Cell culture and maintenance

HeLa cells (human cervix carcinoma,) A549 cells (human lung carcinoma) and HeK293 (human embryonic kidney) cells were obtained from NCCS (National Centre for Cell Sciences, Pune, India). These cell lines were grown in high glucose DMEM with 50 mM glutamine, supplemented with 10% FBS, 100 U/ml penicillin and 100 mg/ml streptomycin. Cells were maintained in a humidified 5% CO_2 incubator at 37 °C.

2.3.2. MTT assay for cytotoxicity

HeLa (human cervix carcinoma), A549 (human lung carcinoma) and Hek293 (human embryonic kidney) cells were seeded in 96-well plates at the density of 1×10^5 cells/well in DMEM media supplemented with 10% FBS. Cells were incubated at 37 °C in 5% CO_2 incubator. Cells were treated with different concentrations (0.5, 2, 4 μg/μl) of INPs and CSO-INPs respectively for 24, 48 and 72 h at 37 °C. 10 μl of MTT (prepared in 1× PBS buffer) from 5 mg/ml stock was added in each well and incubated at 37 °C for 4 h in dark.

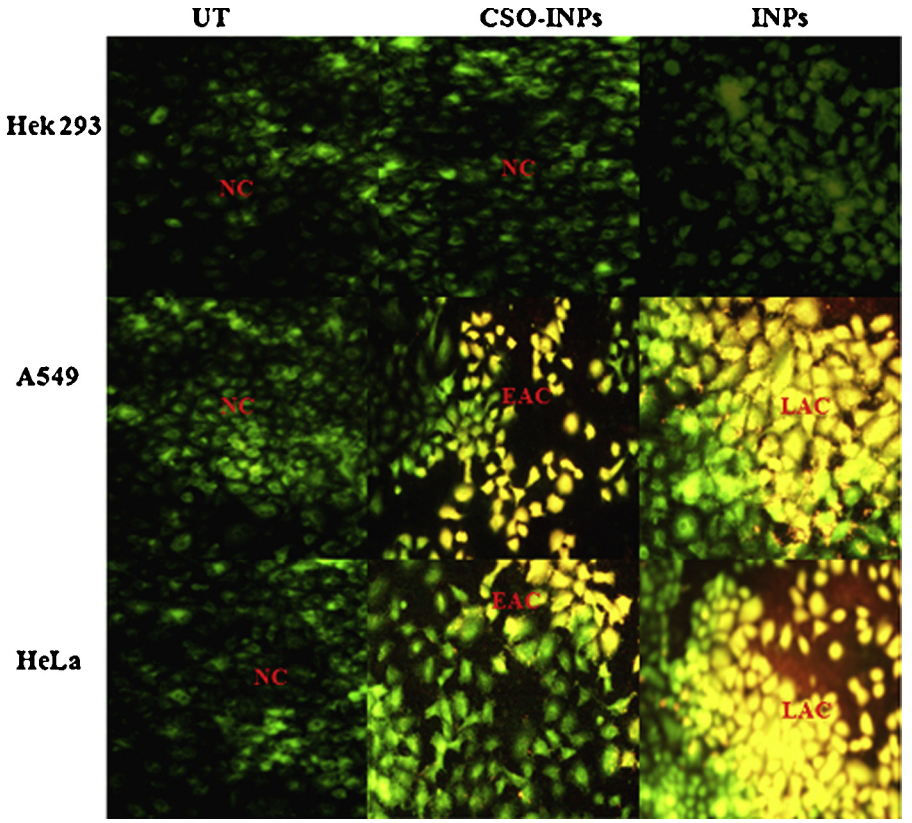

Fig. 7. Acridine orange/ethidium bromide double staining for apoptosis analysis in Hek293, A549 and HeLa cells after iron oxide nanoparticles and chitosan oligosaccharide coated iron oxide nanoparticles (CSO-INPs = 4 μg/μl) treatment at 48 h (UT = untreated, CSO-INPs = chitosan oligosaccharide linked iron nanoparticles, INPs = iron oxide nanoparticles, NC = normal cells, EAC = early apoptosis cells, LAC = late apoptosis cells).

The formazan crystals were dissolved using 100 μl of DMSO [25]. Further, the amount of formazan crystal formation was measured as difference in absorbance by Bio-Red 840 ELISA reader at 570 nm and 690 nm reference wavelength.

2.3.3. Acridine orange/ethidium bromide doubles staining (AO/EB) assay

HeLa, A549 and Hek293 (1×10^5 cells/well) cells were grown on cover slips and treated with 4 μg/μl iron oxide nanoparticles (INPs) and chitosan oligosaccharide coated iron oxide nanoparticles (CSO-INPs) respectively. Cells were incubated in CO_2 incubator at 37 °C for 48 h. Cells were washed with 1× PBS buffer (pH 7.4), fixed with absolute methanol for 10 min, and washed again with 1× PBS buffer (pH7.4). Now, cells were stained with 1 μl of AO/EB cocktail (AO/EB 100 μg/ml) for 10–15 min, cells were then immediately washed with phosphate buffer, followed by imaging using fluorescence microscope [26].

2.3.4. Mitochondria deformation evaluation by transmission electron microscope (TEM)

For the mitochondria morphological alteration analysis, HeLa, A549 and Hek293 cells (1×10^5 cells/well) were treated with 4 μg/μl iron oxide nanoparticles and chitosan oligosaccharide coated iron oxide nanoparticles (CSO-INPs) respectively for 48 h. Cells were trypsinized with 1× trypsin–EDTA followed by centrifugation and fixation with 2% glutaraldehyde in 0.1 sodium cacodylate for 1 h at 4 °C. Cells were washed twice with 0.1 M sodium cacodylate (pH 7.4) and fixed with 2% osmium tetroxide in 0.1 M sodium cacodylate for 1 h at room temperature. Cells were washed again with 1× PBS buffer (pH 7.4). Cells were treated with 1% uranyl acetate for 1 h and washed with 1× PBS buffer (pH 7.4) twice. After fixing and sectioning, cells were dehydrated *via* ethanol and stained with 5% uranyl acetate for 30 min followed by Reynold's lead citrate incubation [27]. Stained cells were examined under JEOL 2100F transmission electron microscope. The presence of INPs and CSO-INPs in mitochondria surface and matrix was further confirmed by the TEM-EDS elemental analysis (TEM, *JEOL 2100F*).

2.3.5. Detection of mitochondria membrane integrity

For apoptosis analysis HeLa, A549 and Hek293 cells were seeded at the density of 1×10^5 cells/well and incubated at 37 °C for 24 h. Cells were treated with 4 μg/μl of INPs and CSO-INPs respectively for 48 h. Cells were trypsinized using 1× trypsin–EDTA and pooled in 1.5 ml tube, washed with 1× PBS buffer. Cells were resuspended in 500 μl of 1× Annexin binding buffer [10× buffer composition: 0.1 M Hepes/NaOH (pH 7.4), 1.4 M NaCl, 25 mM $CaCl_2$], 1 μl of Annexin V-FITC reagent used from stock

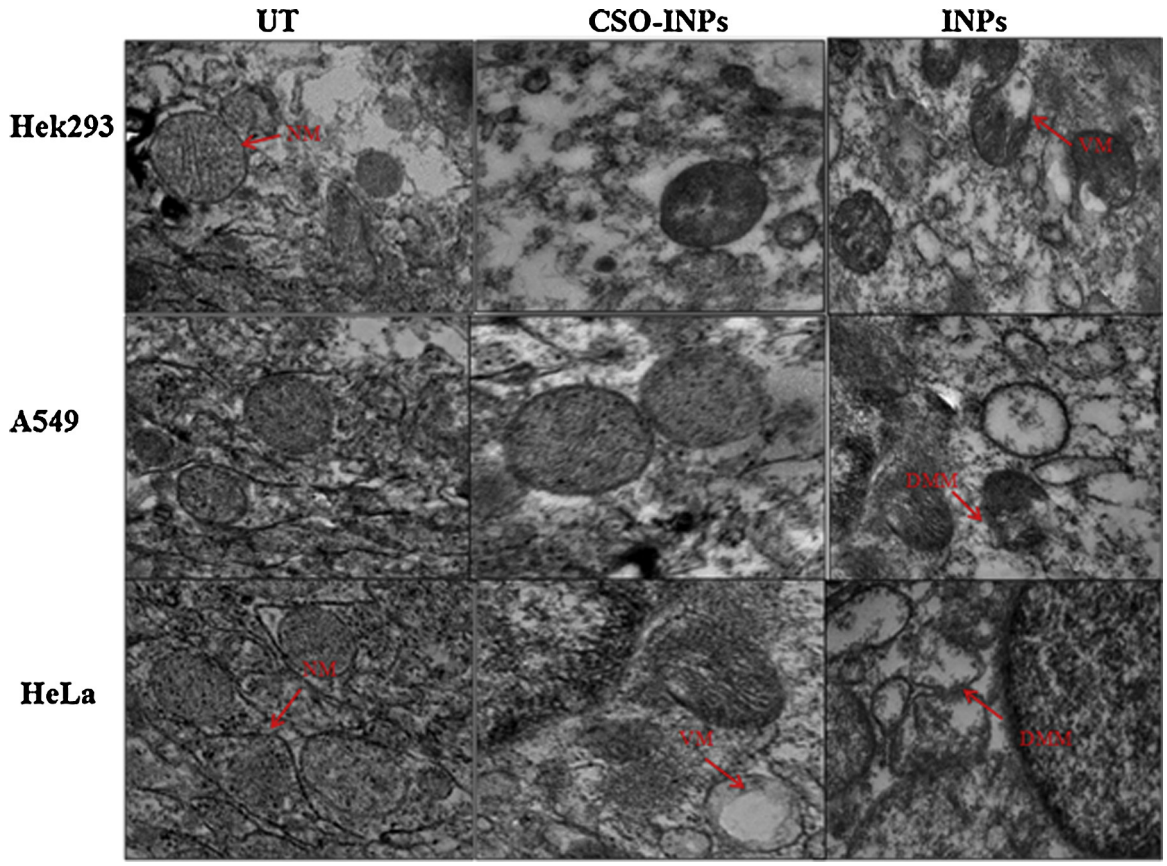

Fig. 8. Morphological alteration of mitochondria after iron oxide nanoparticles (INPs) and chitosan oligosaccharide coated iron oxide nanoparticles (CSO-INPs) treatment in Hek293, A549 and HeLa cells with 4 μg/μl at 48 h (UT = untreated, CSO-INPs = chitosan oligosaccharide linked iron oxide nanoparticles, INPs = iron oxide nanoparticles, NM = normal mitochondria, VM = vesicular mitochondria, DMM = disintegrated mitochondrial membrane).

(final concentration 1 μg/ml). Stained samples were gently mixed and incubated at 37 °C for 10–20 min in dark [28]. FL1 channel was applied for detecting Annexin V-FITC staining through flow cytometry (BD Biosciences) with excitation wavelength 488 nm. Fluorescence spectra were analyzed by FCS 4 Express Flow Cytometry software.

2.3.6. Estimation of mitochondrial membrane potential

Mitochondrial membrane potential was analyzed by JC-1 probe (5,5,6,6-tetrachloro-1,1,3,3-tetraethylbenzimidazolylcarbocyanine iodide) staining [29,30]. HeLa, A549 and Hek293 cells (1×10^5 cells/well) were harvested after 48 h exposure of 4 μg/μl iron oxide nanoparticles and chitosan oligosaccharide coated iron oxide nanoparticles (CSO-INPs) and centrifuged at 400 × *g* for 5 min. Cell pellet was resuspended in 0.5 ml of JC-1 solution (10 μg/ml) for 10 min. Cells were washed with 1× PBS buffer. Mitochondrial depolarization is identified by reduction of the red/green fluorescence ratio. Green fluorescence (monomers) was observed through FL1 channel with almost 10,000 events of each sample using flow cytometry (BD Biosciences) with excitation at 488 nm wavelength. Fluorescence spectra were analyzed by FCS 4 Express Flow Cytometry software.

2.3.7. Measurement of reactive oxygen species (ROS) by DCFH-DA

Analysis of ROS production was carried out using the method reported by Mancini et al. [31], with slight modification. HeLa, A549 and Hek293 cells (1×10^5 cells/well) were seeded and incubated at 37 °C in CO_2 incubator for 24 h. The cells were treated with 4 μg/μl iron oxide nanoparticles (INPs) and chitosan oligosaccharide coated iron oxide nanoparticles (CSO-INPs) respectively for 48 h. Cells were trypsinized with 1× trypsin–EDTA, and centrifuged at 1000 rpm for 5 min. Cells were washed twice with 1× PBS buffer (pH 7.4) followed by 1 h incubation in DCFH-DA (10 μmol/l) in FBS-free DMEM medium. Cells were resuspended in 1× PBS buffer, subjected to flow cytometry analysis. Finally, fluorescence spectrum was measured by flow cytometry (BD Biosciences) at 488 nm excitation and emission at 530 nm wavelength for DCFDA with 10,000 events of each sample. Fluorescence spectra were analyzed by FCS 4 Express Flow Cytometry software.

2.3.8. Measurement of reactive oxygen species (ROS) production by DHE

For further evaluation of ROS production, HeLa, A549 and Hek293 cells (1×10^5 cells/well) were seeded into 24-well plates and allowed to adhere in 24 h. After 24 h,

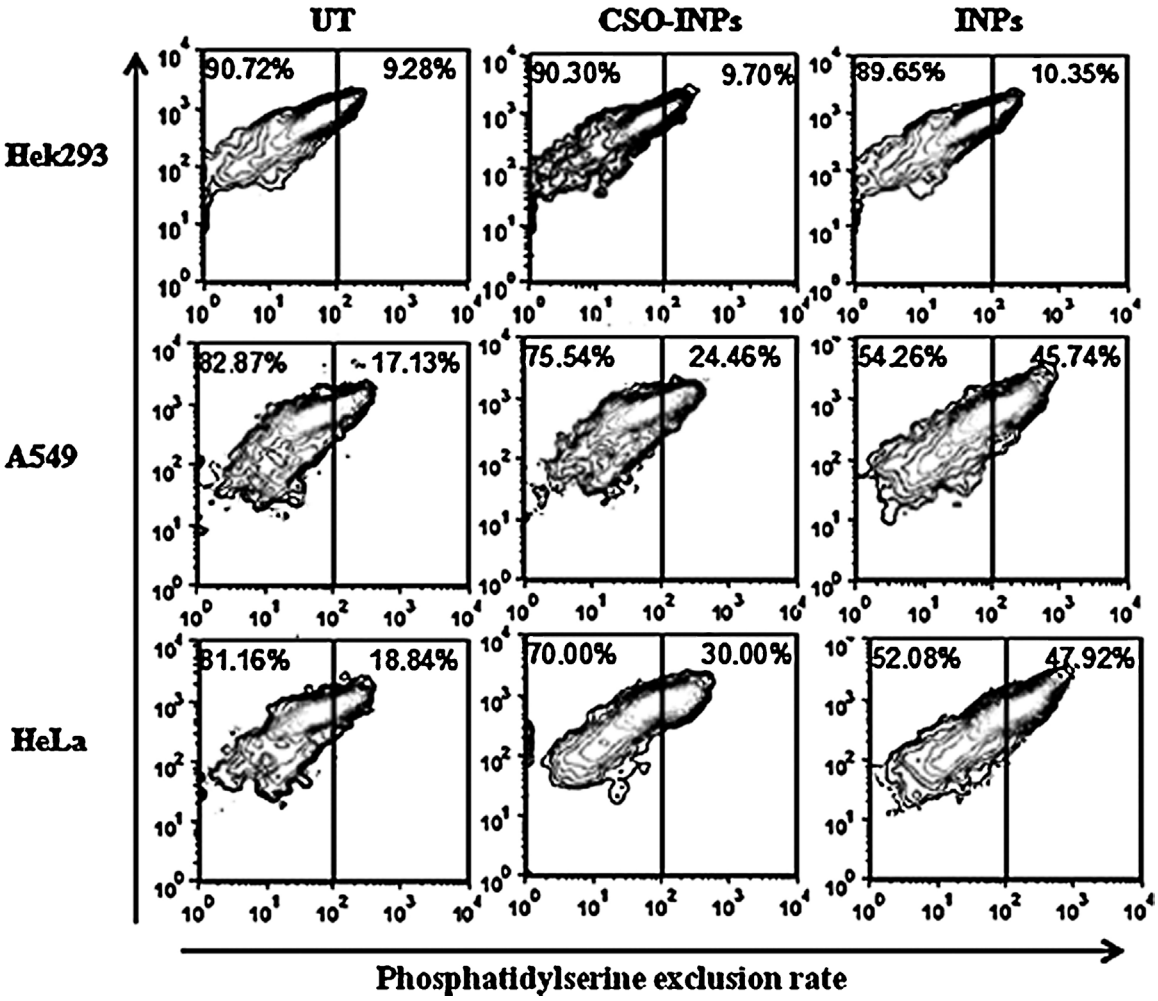

Fig. 9. Phosphatidylserine exclusion illustration by Annexin-V-FITC after iron oxide nanoparticles (INPs) and chitosan oligosaccharide coated iron oxide nanoparticles (CSO-INPs) treatment in Hek293, A549 and HeLa cells with 4 μg/μl at 48 h (UT = untreated, CSO-INPs = chitosan oligosaccharide linked iron oxide nanoparticles, INPs = iron oxide nanoparticles).

fresh media was supplemented with 4 μg/μl iron oxide nanoparticles and chitosan oligosaccharide coated iron oxide nanoparticles (CSO-INPs) respectively. Cells were trypsinized with 1× trypsin–EDTA, and centrifuged at 1000 rpm for 5 min. Cells were washed twice with 1× PBS buffer. Cells were re-suspended in HBSS (Hanks' balanced salt solution) buffer containing the fluorescence probes DHE (2.5 μM). Cells were incubated at 37 °C for 20–30 min in dark and washed with 1× PBS buffer [29]. Finally, fluorescence spectrum was measured by flow cytometry (BD Biosciences) at 488 nm excitation and emission at 620 nm wavelength with 10,000 events of each sample. Fluorescence spectra were analyzed by FCS 4 Express Flow Cytometry software.

2.4. Statistical analysis

Significance of the toxicity of iron oxide nanoparticles (INPs) and chitosan oligosaccharide coated iron oxide nanoparticles (CSO-INPs) in MTT assay was analyzed by Student's *t*-test. Each experiment, with six in replicates, was performed in at least three independent cell culture preparations. The *t*-test was used to evaluate the difference in means between groups with a conventional threshold *p*-value for statistical significance defined as $^{*}p < 0.05$.

3. Results

3.1. Characterization of synthesized INPs and CSO-INPs

Synthesized Fe_3O_4 nanoparticles were found to be monodisperse and spherical in shape having a mean diameter of 6 ± 1.2 nm in Fig. 1(a). The TEM image of Fe_3O_4-chitosan nanoparticles (CSO-INPs) has been shown in Fig. 1(b). The structures of chitosan oligosaccharide coated iron oxide nanoparticles were observed bigger in size with a mean diameter of 8 ± 2.7 nm. TEM image clearly indicates that the surface modification process did not cause significant change in the size of the particles. However, a little aggregation was observed in the Fe_3O_4-CSO nanoparticles, this may be due to higher molecular weight of chitosan oligosaccharide used for the synthesis [22,32,33]. Fig. 2(a)

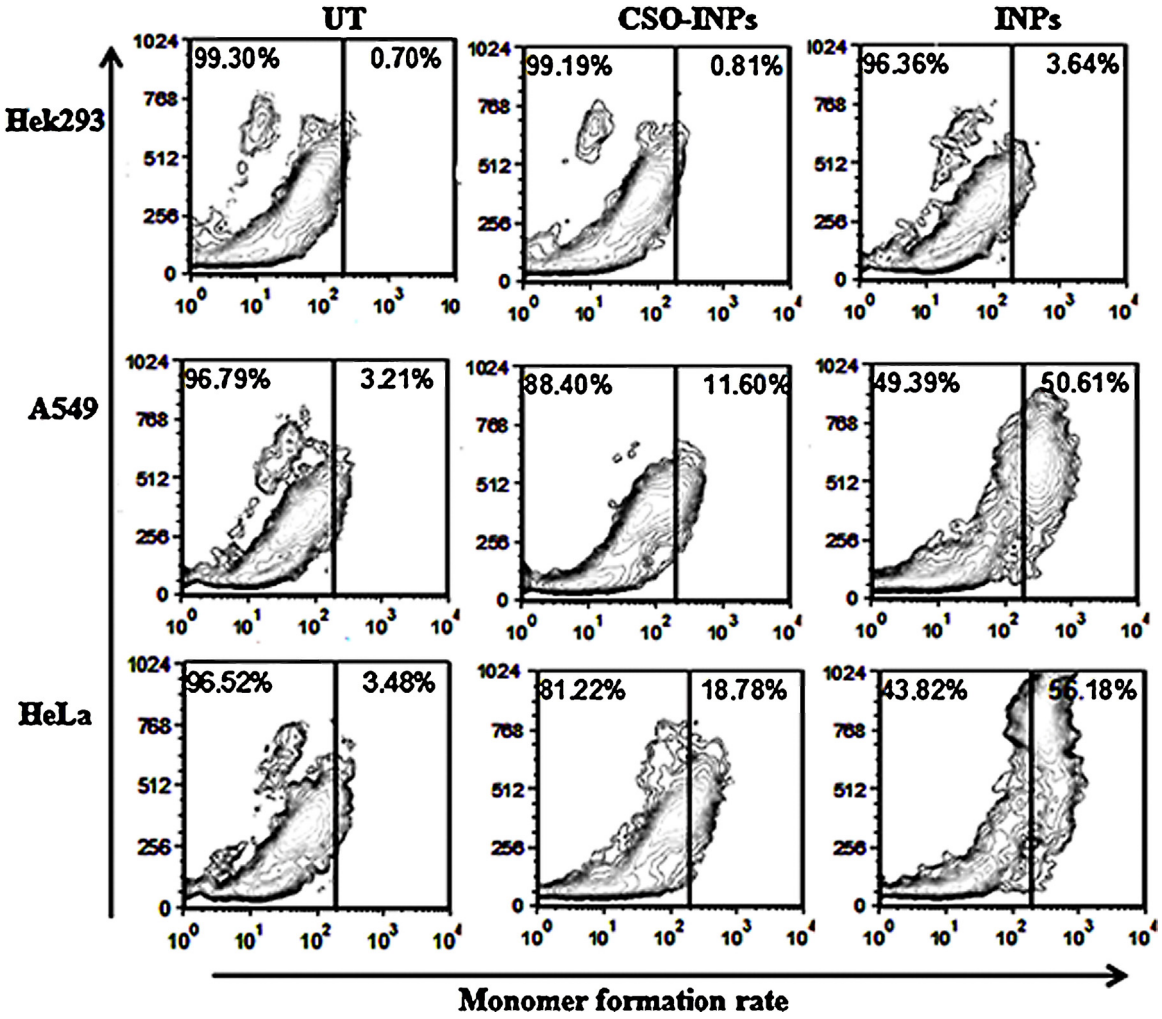

Fig. 10. Mitochondrial membrane potential determination by JC-1 probe after iron oxide nanoparticles (INPs) and chitosan oligosaccharide coated iron oxide nanoparticles (CSO-INPs) treatment in Hek293, A549 and HeLa cells with 4 μg/μl at 48 h (UT = untreated, CSO-INPs = chitosan oligosaccharide linked iron oxide nanoparticles, INPs = iron oxide nanoparticles).

shows X-ray diffraction (XRD) pattern of synthesized iron nanoparticles exhibiting peaks at 2θ at 30.1, 35.5, 42.6, 53.6, 57.0 and 62.8 which can be assigned to diffraction of the (2 2 0), (3 1 1), (4 0 0), (4 2 2), (5 1 1), and (4 4 0) planes, respectively of spinal structured magnetite nanoparticles (JCPDS card no. 82-1533). It is to be noted that the coating process did not result in the phase change of Fe_3O_4. The broad reflection planes can be attributed to the nanosize of the iron oxide nanoparticles [34]. The XRD pattern CSO-INPs exhibited its two characteristic peaks at $2\theta = 20.1, 30.1$, 35.5 and 62.8 in Fig. 2(b). Presence of characteristic peak at $2\theta = 20.1$ for chitosan oligosaccharide along with $2\theta = 30.1$, 35.5 and 62.8 associated with the iron oxide nanoparticles confirms the coating of chitosan oligosaccharide on iron oxide nanoparticles [8,35].

FTIR graph indicates the characteristic peaks of oleic acid coated iron oxide nanoparticles in Fig. 3(a). The $-CH_2$ stretch is seen at 2846 cm^{-1} and 2924 cm^{-1}, C=C at 1645 cm^{-1}, and $-CH_3$ stretching at 1462 cm^{-1}, indicating the presence of oleic acid on nanoparticles surface. Successful amide formation between amine groups in CSO and the carboxylic group of silane was confirmed by the appearance of characteristic bands such as —OH group at 3352 cm^{-1}, C=O (secondary amide formation) at 1635 cm^{-1} and C—O—C at 1095 cm^{-1}, for CSO in Fig. 3(b) [8,22,23,35].

PPMS magnetometer results showed magnetization properties as a function of applied field at 300 K obtained for dry powders of iron oxide nanoparticles and CSO coated iron oxide nanoparticles. The results indicate superparamagnetic behaviour of synthesized nanoparticles, that is, net magnetization of the particles in the absence of an external magnetic field was found to be zero [6]. Fig. 4 shows that the saturation magnetization of the CSO coated sample (12 emu per g) is lower than that of the iron nanoparticles (32 emu per g).

Zeta potential data in Fig. 5(a) shows the zeta potential of INPs coated with silane COOH. The particles consist

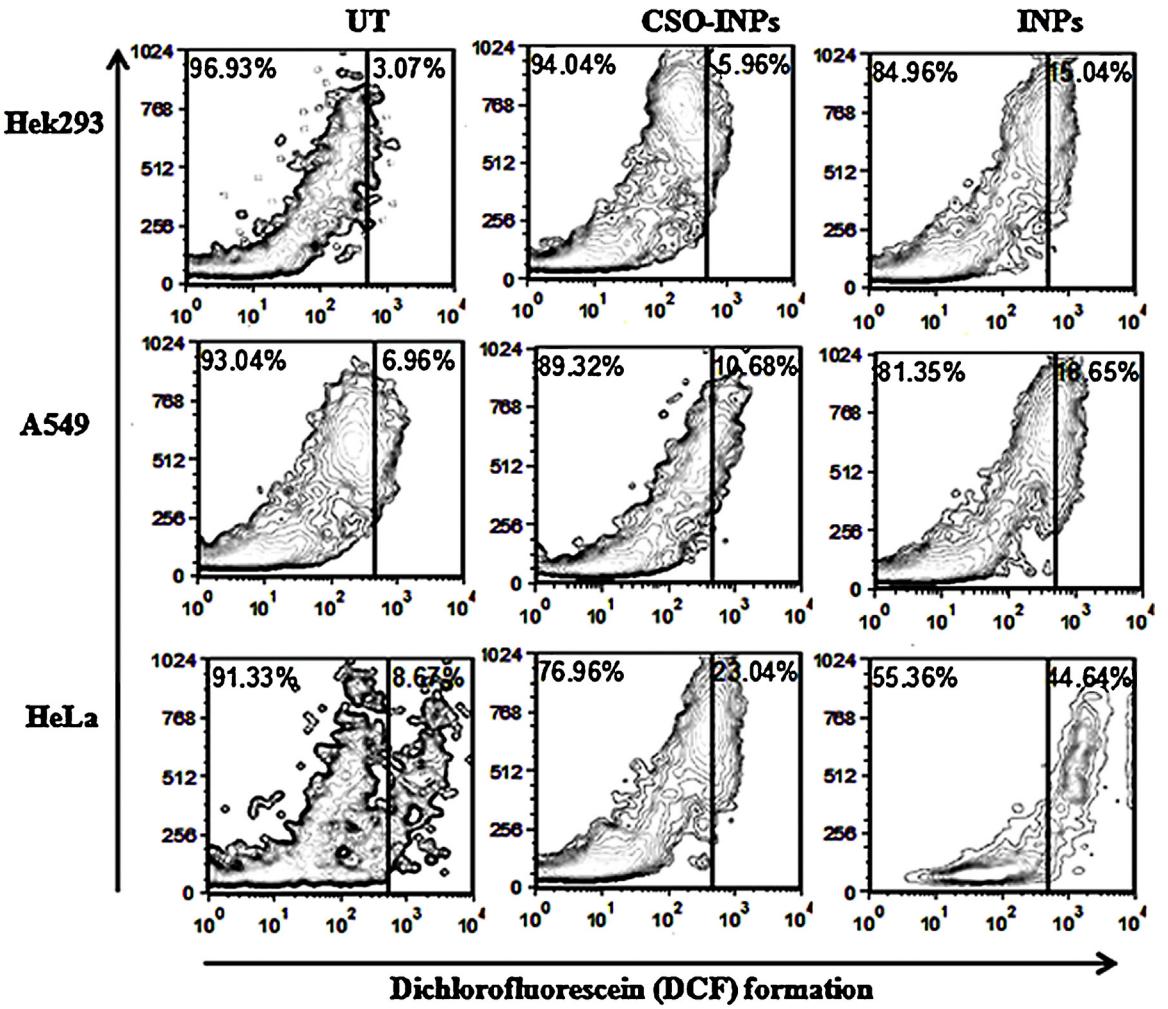

Fig. 11. ROS estimation by dihydrochlorofluorescein-diacetate (DCFH-DA) in Hek293, A549 and HeLa cells after ironoxide nanoparticles (INPs) and chitosan oligosaccharide coated iron oxide nanoparticles (CSO-INP) treatment with 4 μg/μl at 48 h (UT = untreated, CSO-INPs = chitosan oligosaccharide linked iron oxide nanoparticles, INPs = iron oxide nanoparticles).

of zeta potential −1.9, −36.5 and −51 mV at pH 3, 7 and 9 respectively, which may be attributed to negative charge on surface of nanoparticles due to the presence of —COOH group of oleic acid and carboxylic silane surface coating. Zeta potential data in Fig. 5(b) indicates that CSO-INPs were positively charged with a surface potential greater than +37 mV at pH 3. This confirms the presence of amino groups on the nanoparticle surface in their protonated form, and thus establishing the presence of chitosan oligosaccharide on the particle surface. Results indicate that with an increase of pH, the surface charge of the particle decreased which was probably due to the deprotonation tendency of the surface exposed amino groups at higher values of pH [22]. Fig. 5(b) also shows that particles possess positive zeta potential of +11 mV at pH 7, which corresponds to the pH of natural water. However, at pH 9, particles show a negative zeta potential of −2.8 mV.

These results confirm that the nanoparticles have sufficient colloidal stability which is necessary for biological and environmental applications [8].

3.2. Toxicity analysis of synthesized INPs and CSO-INPs

3.2.1. MTT assay for cytotoxicity analysis

MTT (3-(4,5-dimethylthiazol-2yl)-2,5-diphenyltetrazolium) assay for viability of various cell lines was performed. The assay is based on reduction of soluble yellow tetrazolium into insoluble purple formazan crystals by mitochondrial succinate dehydrogenase of viable cell. Therefore, the rate of formazan crystal formation is directly proportional to number of viable cells which is measured in terms of absorbance [25]. The results in Fig. 6 clearly indicate that the toxic effect of CSO-INPs on A549 and HeLa cells were moderate as compared to bare INPs treatment. Higher toxicity of iron oxide nanoparticles could be attributed to high release of iron ions in intracellular space and *in situ* degradation [19]. This toxicity of nanoparticles was found to be time and dose dependent. Results clearly indicate that the cell viability decreased with increase in dose and time. In case of Hek293 cells iron oxide nanoparticles lead to toxic effects whereas,

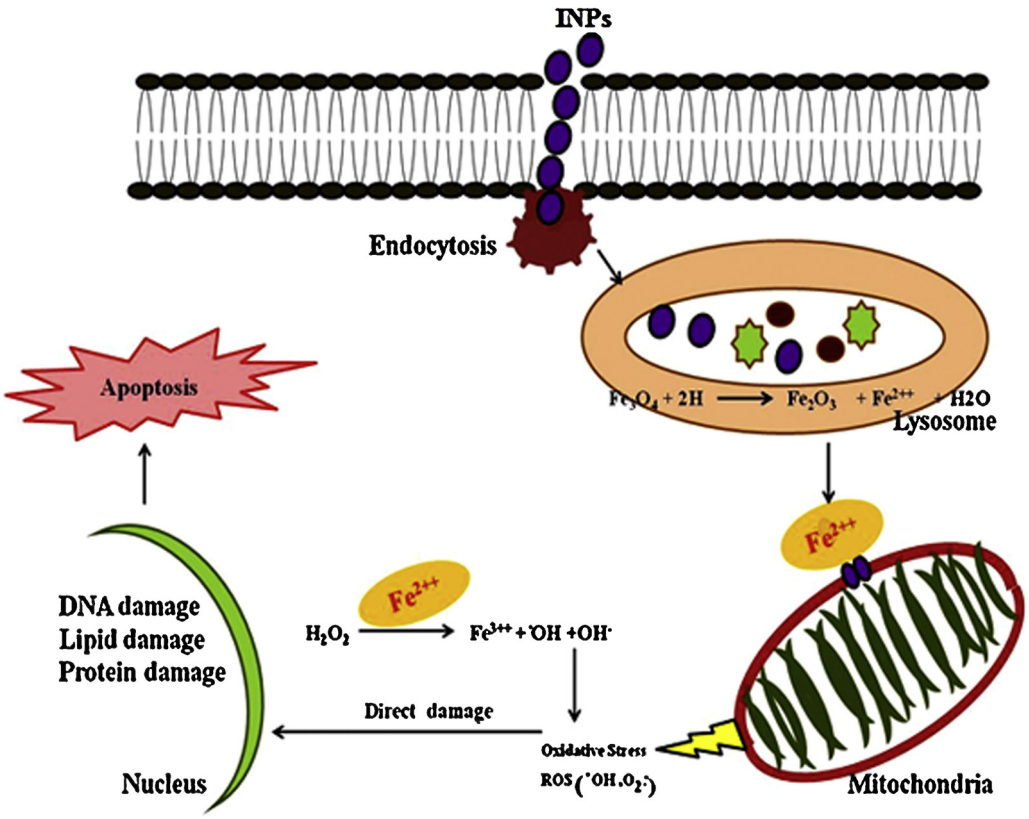

Fig. 12. Schematic representation of intracellular uptake pathways and targets of INPs.

CSO-INPs did not cause any significant toxicity. All findings clearly suggest that the chitosan oligosaccharide coating reduces the toxic effects of INPs. Less toxicity of CSO-INPs may be attributed to controlled release of Fe^{2+} ions, which trigger the ROS mediated cell death [17,19].

3.2.2. Morphological alteration analysis by AO/EB staining and TEM

To compare the apoptotic effects on non-cancerous and cancer cell lines, cells were subjected to INPs and CSO-INPs treatment followed by Acridine orange/ethidium bromide double staining (AO/EB). Acridine orange dye stains both live and dead cells. While ethidium bromide, a DNA binding dye, stains those cells that have lost nuclear membrane integrity. Mixture of both dyes is commonly used to visualize nuclear membrane disintegration and apoptotic body formation that are characteristic of apoptosis. Three kinds of cells were observed as per the fluorescence emission spectra. (i) Normal cells appeared in organized structure with an intact nuclei stained with green fluorescence. (ii) Early apoptotic cells were visible with bright green and light orange patches; and (iii) Late apoptotic cells which were stained with orange to red patches [26]. After treatment with iron oxide nanoparticles, cells exhibit orange colour with some patches of red, indicating early and late phase of apoptosis whereas, this kind of colour distribution was rarely seen in chitosan oligosaccharide coated iron oxide nanoparticles (CSO-INPs) treated cells in Fig. 7. The results revealed that CSO-INPs caused less apoptosis in healthy as well as cancer cell lines as compared to uncoated/bare INPs.

TEM image in Fig. 8 suggests that the INPs treatment induces remodelling of inner mitochondrial membrane and subsequent lost of membrane integrity of mitochondria in HeLa and A549 cells. Moreover, moderate alternation was observed in case of Hek293 cells. TEM images clearly indicate that the CSO-INPs cause moderate deformation in mitochondria compared to INPs treatment. As we know mitochondria of healthy cells have intact outer membrane and organized cristae as compared to the cells undergoing apoptosis, while alteration in mitochondria appears during late apoptosis phase and is generated due to loss of mitochondrial membrane potential and release of cytochrome c resulting to expansion of mitochondrial matrix and ruptured outer membrane [27].

Results of TEM-EDX elemental analysis of INPs treated cells clearly demonstrate the prominent presence of elemental iron, silicon and oxygen (components of INPs) in mitochondrial membrane as well as in mitochondrial matrix (Supplementary Fig. S1). In contrast, elemental analysis of CSO-INPs treated mitochondria shows the presence of lesser amount of iron with nitrogen, silica and oxygen (component of CSO-INPs) (Supplementary Fig. S2). These findings clearly indicate the controlled release of iron ion by the chitosan oligosaccharide coating of CSO-INPs,

therefore, inducing lesser cellular toxicity in the case of CSO-INPs treated cells.

3.3. Assessment of apoptosis pathway

3.3.1. Evaluation of mitochondria membrane integrity

Apoptosis is responsible for multiple alterations in mitochondrial membrane. During apoptosis, mitochondrial phosphatidylserine is externalized from inner surface to the outer surface. Apoptosis is measured in terms of binding of externalized phosphatidylserine to phospholipid binding protein Annexin V conjugated with fluorochromes [28]. Fig. 9 shows that the CSO-INPs treatment causes moderated disintegration in mitochondrial membranes of HeLa, A549 and Hek293 cells as compared to the bare INPs. This data highlights the fact that chitosan coating of iron oxide nanoparticles reduces its apoptotic triggering effects through lesser disintegration of mitochondrial membrane integrity.

3.3.2. Mitochondrial membrane potential analysis

The loss of mitochondrial membrane potential, a distinctive feature of apoptotic cell, is analysed by cationic carbocyanine dye JC-1. In a normal cell, JC-1 dye is present in monomeric form in cytosol and emits green fluorescence, and accumulate as aggregates in mitochondria emitting red fluorescence. Whereas in mitochondrial membrane disintegrated apoptotic cell, JC-1 retains its monomeric form in mitochondria and emits green fluorescence only [29,30].

Treatment of iron oxide nanoparticles progressively dissociates mitochondrial potential and increases JC-1 green fluorescence without a corresponding increase in JC-1 red fluorescence in HeLa, A549 and Hek293 cells, whereas moderate JC-1 red fluorescence was observed in CSO-NPs treated cells in Fig. 10. Thus results suggest that the formation of monomer of JC-1 is high in iron oxide nanoparticles treated HeLa, A549 and Hek293 cells, with respect to CSO-NPs indicating that INPs toxicity may be reduced due to coating of chitosan oligosaccharide.

3.3.3. Analysis of ROS generation by dihydrochlorofluorescein-diacetate (DCFH-DA) and dihydroethidine (DHE)

DCFH-DA assay for ROS generation analysis revealed that Dichlorofluorescein (DCF) production is high in iron oxide nanoparticles treated Hek293, A549 and HeLa cells with respect to CSO-INPs treated cells in Fig. 11. Production of highly fluorescent DCF in INPs treated cells may be attributed to the oxidation of non-polar dye DCFH-DA by apoptosis induced intracellular ROS and other peroxides. In a non-apoptotic cell DCFH-DA converts to its non-fluorescent, non-polar derivative DCFH by the action of cellular esterase [36].

Dihydroethidine (HE) probe is oxidized into red fluorescent product ethidium in the presence of superoxide anion. This action has been associated with mitochondrial uncoupling and increased ROS production [31]. Interaction of ethidium to DNA is inferred with higher red fluorescence in INPs treated cell compared to CSO-INPs treated HeLa, A549 and Hek293 cells in Fig. S3 (Supplementary data). This finding also demonstrates that the ROS production increases in dose and time-dependent manner after treatment of iron oxide nanoparticles and chitosan oligosaccharide coated iron oxide nanoparticles (CSO-INPs).

Therefore, this correlation is maintained with JC-1 monomer formation and continuous enhancement of ROS production, these features are indicators of programmed cell death [37]. The conclusion of this study strongly corroborates that the toxicity effect of CSO-INPs was probably reduced due to covering of chitosan oligosaccharide on bare iron oxide nanoparticles.

The findings of the present study also indicate the probable mechanism of nanoparticles interaction with various cellular targets resulting in cytotoxicity and it also corroborates with the earlier established hypothesis in Fig. 12 [15–17,19,38].

It is hypothesized that internalized nanoparticles release ferrous form of iron ion after the enzymatic degradation of INPs into the acidic environment of lysosome. Ferrous ion could react with hydrogen peroxide generated in the mitochondria and induces the generation of highly reactive oxygen species as hydroxyl radicals through the Fenton reaction [16,19,38,39]. Induced ROS further causes the inflammation in the cell, interfering mitochondrial function and release of cytochrome c by altered membrane potential which ultimately triggers the apoptosis [37].

Findings of the current study indicate that surface engineering of iron oxide nanoparticles with chitosan oligosaccharide reduces cytotoxicity of bare iron oxide nanoparticles. Our results indicate that the chitosan oligosaccharide coating on INPs results in the decrease in cellular damage including lesser damage to mitochondrial membrane and moderate ROS production. The reduced toxicity of INPs after the coating of polycationic chitosan oligosaccharide may be attributed to controlled release of Fe^{2+} ion from nanoparticles into acidic environment of lysosomes, which is a key factor in the toxicity determination [17,40,41].

4. Conclusion

Iron oxide nanoparticles (INPs) and chitosan oligosaccharide linked iron oxide nanoparticles (CSO-INPs) were synthesized for evaluation of their *in vitro* toxicity. Synthesized iron oxide nanoparticles were found to be well dispersed and non-agglomerative. 3-(4,5-dimethylthiazol-2-yl)-2,5-diphenyltetrazolium bromide (MTT) assay along with flow cytometry study for cell viability, membrane integrity, mitochondrial membrane potential (MMP), and reactive oxygen species (ROS) assays clearly indicated the toxicity potential of INPs. Coating of these INPs with biocompatible chitosan oligosaccharide not only makes these nanoparticles soluble in aqueous environment over a range of pH but less toxic also. Present study also suggests the need of comprehensive *in vivo* toxicity assessment for the critical dose evaluation of surface engineered iron oxide nanoparticles.

Conflict of interest

Nothing to declare.

Transparency document

The Transparency document associated with this article can be found in the online version.

Acknowledgements

Sudeep Shukla, one of the authors of the present manuscript, was recipient of fellowship from Council of Scientific and Industrial Research (CSIR). We are thankful to Dr. Aparna Dixit and her research group for their help in flow cytometry data analysis. We are also thankful to Advance Instrumentation Facility (AIRF), JNU, New Delhi for various analytical instruments used in this work.

Appendix A. Supplementary data

Supplementary data associated with this article can be found, in the online version, at doi:10.1016/j.toxrep.2014.11.002.

References

[1] K. Donaldson, V. Stone, C.L. Tran, W. Kreyling, P.J. Borm, Nanotoxicology, Occup. Environ. Med. 61 (2004) 727–728.
[2] W.-T. Liu, Nanoparticles and their biological and environmental applications, J. Biosci. Bioeng. 102 (2006) 1–7.
[3] M.C. Roco, National Nanotechnology Initiative – Past, Present, Future. Handbook on Nanoscience, Engineering, and Technology, 2nd ed., 2007, pp. 1–42.
[4] A.-H. Lu, E.L. Salabas, F. Schüth, Magnetic nanoparticles: synthesis, protection, functionalization, and application, Angew. Chem. Int. Ed. Engl. 46 (2007) 1222–1244.
[5] S. Laurent, D. Forge, M. Port, A. Roch, C. Robic, L. Vander Elst, R.N. Muller, Magnetic iron oxide nanoparticles: synthesis, stabilization, vectorization, physicochemical characterizations, and biological applications, Chem. Rev. 108 (2008) 2064–2110.
[6] L. Zhang, R. He, H.-C. Gu, Oleic acid coating on the monodisperse magnetite nanoparticles, Appl. Surf. Sci. 253 (2006) 2611–2617.
[7] M. Rinaudo, Chitin and chitosan: properties and applications, Prog. Polym. Sci. 31 (2006) 603–632.
[8] G. Unsoy, S. Yalcin, R. Khodadust, G. Gunduz, U. Gunduz, Synthesis optimization and characterization of chitosan-coated iron oxide nanoparticles produced for biomedical applications, J. Nanopart. Res. 14 (2012) 964.
[9] V.K. Mourya, N.N. Inamdar, Chitosan-modifications and applications: opportunities galore, React. Funct. Polym. 68 (2008) 1013–1051.
[10] P.J.A. Borm, D. Robbins, S. Haubold, T. Kuhlbusch, H. Fissan, K. Donaldson, R. Schins, V. Stone, W. Kreyling, J. Lademann, J. Krutmann, D. Warheit, E. Oberdorster, The potential risks of nanomaterials: a review carried out for ECETOC, Part. Fiber Toxicol. 3 (2006) 11.
[11] A. Maynard, R.J. Aitken, T. Butz, V. Colvin, K. Donaldson, G. Oberdörster, M.A. Philbert, J. Ryan, A. Seaton, V. Stone, S.S. Tinkle, L. Tran, N.J. Walker, D.B. Warheit, Safe handling of nanotechnology, Nature 444 (2006) 267–269.
[12] G. Oberdörster, E. Oberdörster, J. Oberdörster, Nanotoxicology: an emerging discipline evolving from studies of ultrafine particles, Environ. Health Perspect. 113 (2005) 823–839.
[13] K. Savolainen, H. Alenius, H. Norppa, L. Pylkkänen, T. Tuomi, G. Kasper, Risk assessment of engineered nanomaterials and nanotechnologies – a review, Toxicology 269 (2010) 92–104.
[14] B. Szalay, Iron Oxide Nanoparticles and their Toxicological Effects: In Vivo and In Vitro Studies, University of Szeged, 2012, pp. 1–24.
[15] M. Mahmoudi, H. Hofmann, B. Rothen-Rutishauser, A. Petri-fink, Assessing the in vitro and in vivo toxicity of superparamagnetic iron oxide nanoparticles, Chem. Rev. 112 (2012) 2323–2338.
[16] M. Mahmoudi, A. Simchi, A.S. Milani, P. Stroeve, Cell toxicity of superparamagnetic iron oxide nanoparticles, J. Colloid Interface Sci. 336 (2009) 510–518.
[17] M.A. Malvindi, V. De Matteis, A. Galeone, V. Brunetti, G.C. Anyfantis, A. Athanassiou, R. Cingolani, P.P. Pompa, Toxicity assessment of silica coated iron oxide nanoparticles and biocompatibility improvement by surface engineering, PLOS ONE 9 (2014) e85835.
[18] U.O. Hafeli, J.S. Riffle, L. Harris-shekhawat, A. Carmichael-baranauskas, F. Mark, J.P. Dailey, D. Bardenstein, Cell uptake and in vitro toxicity of magnetic nanoparticles suitable for drug delivery, Mol. Pharm. 6 (2009) 1417–1428.
[19] N. Singh, G.J.S. Jenkins, R. Asadi, S.H. Doak, Potential toxicity of superparamagnetic iron oxide nanoparticles (SPION), Nano Rev. 1 (2010) 1–15.
[20] N.R. Jana, Y. Chen, X. Peng, Size- and shape-controlled magnetic (Cr, Mn, Fe, Co, Ni) oxide nanocrystals via a simple and general approach, Chem. Mater. 16 (2004) 3931–3935.
[21] R. De Palma, S. Peeters, M.J. Van Bael, H. Rul, Van Den, K. Bonroy, W. Laureyn, J. Mullens, G. Borghs, G. Maes, Silane ligand exchange to make hydrophobic superparamagnetic nanoparticles water-dispersable, Chem. Mater. 19 (2007) 1821–1831.
[22] A. López-Cruz, C. Barrera, V.L. Calero-DdelC, C. Rinaldi, Water dispersible iron oxide nanoparticles coated with covalently linked chitosan, J. Mater. Chem. 19 (2009) 6870–6876.
[23] L. Huang, X. Cheng, C. Liu, K. Xing, J. Zhang, G. Sun, X. Li, X. Chen, Preparation, characterization, and antibacterial activity of oleic acid-grafted chitosan oligosaccharide nanoparticles, Front. Biol. China 4 (2009) 321–327.
[24] G.H. Woehrle, J.E. Hutchison, S. Ozkar, R.G. Frinke, Analysis of nanoparticle transmission electron microscopy data using a public-domain image-processing program, Turk. J. Chem. 30 (2006) 1–13.
[25] R.F. Hussain, A.M.E. Nouri, R.T.D. Oliver, A new approach for measurement of cytotoxicity using colorimetric assay, J. Immunol. Methods 160 (1993) 89–96.
[26] D. Baskić, S. Popović, P. Ristić, N.N. Arsenijević, Analysis of cycloheximide-induced apoptosis in human leukocytes: fluorescence microscopy using Annexin V/propidium iodide versus acridin orange/ethidium bromide, Cell Biol. Int. 30 (2006) 924–932.
[27] M.A. Altinoz, A. Bilir, G. Gedikoglu, E. Ozcan, G. Oktem, M. Muslumanoglu, Medroxyprogesterone and tamoxifen augment anti-proliferative efficacy and reduce mitochondria-toxicity of epirubicin in FM3A tumor cells in vitro, Cell Biol. Int. 31 (2007) 473–481.
[28] C. Schult, M. Dahlhaus, S. Ruck, M. Sawitzky, F. Amoroso, S. Lange, D. Etro, A. Glass, G. Fuellen, S. Boldt, O. Wolkenhauer, L. Neri, M. Freund, C. Junghanss, The multikinase inhibitor sorafenib displays significant antiproliferative effects and induces apoptosis via caspase 3,7 and PARP in B- and T-lymphoblastic cells, BMC Cancer 10 (2010) 1–11.
[29] M. Reers, T.W. Smith, L.B. Chen, J-aggregate formation of a carbocyanine as a quantitative fluorescent indicator of membrane potential, Biochemistry 30 (1991) 4480–4486.
[30] S.T. Smiley, M. Reers, C. Mottola-Hartshorn, M. Lin, A. Chen, T.W. Smith, G.D. Steele, L.B. Chen, Intracellular heterogeneity in mitochondrial membrane potentials revealed by a J-aggregate-forming lipophilic cation JC-1, Proc. Natl. Acad. Sci. U. S. A. 88 (1991) 3671–3675.
[31] M. Mancini, B.O. Anderson, E. Caldwell, M. Sedghinasab, P.B. Paty, D.M. Hockenbery, Mitochondrial proliferation and paradoxical membrane depolarization during terminal differentiation and apoptosis in a human colon carcinoma cell line, J. Cell Biol. 138 (1997) 449–469.
[32] D.T.K. Dung, T.H. Hai, L.H. Phuc, B.D. Long, L.K. Vinh, P.N. Truc, Preparation and characterization of magnetic nanoparticles with chitosan coating, J. Phys. Conf. Ser. 187 (2009) 012036.
[33] G. Li, K. Huang, Y. Jiang, P. Ding, D. Yang, Preparation and characterization of carboxyl functionalization of chitosan derivative magnetic nanoparticles, Biochem. Eng. J. 40 (2008) 408–414.
[34] Y.-C. Chang, D.-H. Chen, Preparation and adsorption properties of monodisperse chitosan-bound Fe_3O_4 magnetic nanoparticles for removal of Cu (II) ions, J. Colloid Interface Sci. 283 (2005) 446–451.
[35] H. Li, Z. Li, T. Liu, X. Xiao, Z. Peng, L. Deng, A novel technology for biosorption and recovery hexavalent chromium in wastewater by bio-functional magnetic beads, Bioresour. Technol. 99 (2008) 6271–6279.
[36] A. Aranda, L. Sequedo, L. Tolosa, G. Quintas, E. Burello, J.V. Castell, L. Gombau, Dichloro-dihydro-fluorescein diacetate (DCFH-DA) assay: a quantitative method for oxidative stress assessment of nanoparticle-treated cells, Toxicol. In Vitro 27 (2013) 954–963.

[37] N. Zamzami, P. Marchetti, M. Castedo, D. Decaudin, A. Macho, T. Hirsch, S.A. Susin, P.X. Petit, B. Mignotte, G. Kroemer, Sequential reduction of mitochondrial transmembrane potential and generation of reactive oxygen species in early programmed cell death, J. Exp. Med. 182 (1995) 367–377.
[38] S.M. Hussain, K.L. Hess, J.M. Gearhart, K.T. Geiss, J.J. Schlager, In vitro toxicity of nanoparticles in BRL 3A rat liver cells, Toxicol. In Vitro 19 (2005) 975–983.
[39] S. Toyokuni, Role of iron in carcinogenesis: cancer as a ferrotoxic disease, Cancer Sci. 100 (2009) 9–16.
[40] M. Lévy, F. Lagarde, V.-A. Maraloiu, M.-G. Blanchin, F. Gendron, C. Wilhelm, F. Gazeau, Degradability of superparamagnetic nanoparticles in a model of intracellular environment: follow-up of magnetic, structural and chemical properties, Nanotechnology 21 (2010) 395103.
[41] K.L.S. Worthington, A. Adamcakova-Dodd, A. Wongrakpanich, I.A. Mudunkotuwa, K.A. Mapuskar, V.B. Joshi, A.C. Guymon, D.R. Spitz, V.H. Grassian, P.S. Thorne, A.K. Salem, Chitosan coating of copper nanoparticles reduces in vitro toxicity and increases inflammation in the lung, Nanotechnology 24 (2013) 395101.